1-2013

A novel 3D3C particle tracking method suitable for microfluidic flow measurements

Craig Snoeyink
Texas Tech University

Steven Wereley
Birck Nanotechnology Center, Purdue University, wereley@purdue.edu

Snoeyink, Craig and Wereley, Steven, "A novel 3D3C particle tracking method suitable for microfluidic flow measurements" (2013). *Birck and NCN Publications.* Paper 1319.
http://dx.doi.org/10.1007/s00348-012-1453-7

Exp Fluids (2013) 54:1453
DOI 10.1007/s00348-012-1453-7

RESEARCH ARTICLE

A novel 3D3C particle tracking method suitable for microfluidic flow measurements

Craig Snoeyink · Steve Wereley

Received: 12 December 2011 / Revised: 19 December 2012 / Accepted: 28 December 2012 / Published online: 12 January 2013

Abstract This article presents a novel method for determining the three-dimensional location of fluorescent particles that is suitable for three-dimensional particle tracking velocimetry measurements in microfluidic flows. This method determines the depth of a particle by inserting a convex lens and axicon into the optical path between a microscope and camera. For particles close to the focal plane, this converts the wavefront from a particle into a Bessel beam, the frequency, and center of which can be directly related to the three-dimensional position of the particle. A robust image analysis method is presented that can determine the properties of the Bessel beam necessary to calculate the particle position. The theory and data analysis method are verified by comparing the calculated position of 1-μm particles to the known position of the particles which scanned through a depth of 100 μm. The average error in the calculated position was 4 μm. Finally, the method is applied to 3D3C particle tracking velocimetry of Poiseuille flow in a 200-μm-deep channel. Uniquely, this method requires no calibration procedure and is insensitive to variations in particle size and brightness.

1 Introduction

As the field of microfluidics has matured, the flows involved have continued to increase in complexity. Manufacturing ever smaller feature sizes has become increasingly easy. In addition, the range of forces available to manipulate particles and fluid flows has grown. What started with pressure or capillary driven flows has exploded into a range of dynamic and powerful forces such as dielectrophoresis, eletrothermophoresis, electrophoresis, acoustophoresis, and others.

Along with new abilities has come the need to measure and visualize the velocity fields within microfluidic devices. Micro-particle image velocimetry (μPIV) first introduced in 1998 quickly became the tool of choice for flow characterization in microfluidics (Santiago et al. 1998; Meinhart et al. 1999). Instead of using a laser sheet, as is common in macroscale PIV, μPIV uses volume illumination with fluorescent particles. As a result, μPIV relies on the relatively thin focal depth of a microscope objective to restrict the imaged particles to the focal plane. The improvement of μPIV and its adaptation to a variety of fields, from biological to chemical and pharmaceutical measurements, is an ongoing process. Reviews of the state of the art for μPIV are published by Lindkin et al. (2009) and Wereley and Meinhart (2010).

Micro-PIV is not without its limitations. Since the technique uses volume illumination, particles that are not in the focal plane still contribute to the image. Flows with high-velocity gradients can exhibit a significant error in what has been termed the depth of correlation problem (Olsen and Adrian 2000). Additionally, the velocity field produced by micro-PIV is a two-dimensional projection of a three-dimensional velocity field. Both of these factors make μPIV ill suited for characterizing complex and three-dimensional microfluidic flows. What is needed and what this paper addresses is a measurement method that can provide three-dimensional flow characterization without errors due to velocity gradients.

C. Snoeyink (✉)
Department of Mechanical Engineering, Texas Tech University, Lubbock, TX, USA
e-mail: craig.snoeyink@ttu.edu

S. Wereley
Department of Mechanical engineering, Birck Nanotechnology Center, Purdue University, West Lafayette, IN, USA

To extend the measurements into the third dimension, several measurement techniques have been developed. For example, volumetric-correlation PIV utilizes the shape of the cross-correlation peak to determine the two-dimensional velocity field as a function of depth (Nguyen et al. 2011). While this is not a fully three-dimensional velocimetry technique, it has the distinct advantage of utilizing the same experimental equipment and data as a traditional μPIV system. In addition, since it is a correlation-based technique, it is capable of handling much higher seed particle concentrations then particle tracking-based methods.

Micro-digital holographic particle tracking velocimetry (micro-DHPTV), introduced in 2005, overcomes many of the limitations of micro-PIV by reconstructing three-dimensional particle locations from digital holograms. The digital holograms are created by shining coherent light through a channel and analyzing the interference patterns produced by light scattered off seed particles as recorded by a digital camera (Satake et al. 2006; Kim and Lee 2007). Since a single beam is used for both the reference and the illumination wave, alignment issues are significantly decreased, and the measurement can be accomplished with equipment common to μPIV measurements (Katz and Sheng 2010; Choi et al. 2012). Micro-DHPTV is also uniquely flexible; it has no requirements on the tracer particles other then that they scatter light. As a result, micro-DHPTV can be used to follow un-tagged biological specimens (Sohn et al. 2010), while micro-DHPTV has seen widespread application but suffers from several drawbacks (Cierpka and Kähler 2011), namely a reduction in seeding density and reduced resolution in the axial direction.

An alternative approach is to slightly modify a traditional micro-PIV experimental setup. Several measurement techniques take this approach and are capable of producing a 3D3C velocity field. The simplest experimental method is to use the defocused and diffracted image of a particle to estimate its distance from the focal plane (Wu et al. 2005). However, using the defocused particle image poses a few problems. It is not always obvious what features of the image to use or how to define them. Additionally, while it is possible to use this technique with very small particles (Speidel et al. 2003), in practice, one must use a dilute suspension of large particles in order to obtain clear particle outlines.

The particle image can also be modified in order to ease the process of determining the particle images radius. Digital defocused micro-particle tracking velocimetry (DDuPTV), introduced in 2005, modifies the defocused image of the particle by putting an aperture with multiple pin holes in the optical path of the microscope (Yoon and Kim 2006). The technique is widely used and capable of diverse measurements such as measuring cardiac cell motion in a living embryo (Lu et al. 2012). The addition of an aperture modifies the particle image, turning it into a set of dots for which the relative spacing is related to the depth of the particle. While this simplifies the analysis of images, the aperture blocks a large portion of the light available from each particle reducing the contrast between the dots and background noise.

An alternative method for modifying the particle image, called astigmatism particle tracking velocimetry (APTV), places a cylindrical lens in between the microscope and camera (Cierpka et al. 2010). The cylindrical lens deforms the particle image into an ellipse where the major and minor axis lengths provide information on the depth of the particle. An advantage of this method is that, unlike other defocusing methods, APTV can self-calibrate using independent measures of the lengths of the two axis of the particle image ellipses (Cierpka et al. 2011). However, APTV, along with the other defocusing methods discussed, generally requires larger particles and dilute suspensions.

The measurement method presented in this article, which we have termed Interference particle tracking velocimetry (Interference-PTV), determines the depth of the particle in a fundamentally different way. Whereas most 3D particle locating techniques rely on correlating some form of deformation of the particle image to the particle's distance from the focal plane, Interference-PTV technique measures the direction and curvature of the wavefront produced by a particle. The curvature of the wavefront can then be directly related to the position of the particle using paraxial optics.

Measuring the curvature and direction of the wavefront is accomplished by placing an axicon between the camera and imaging optics (McLeod 1954). An axicon is an unique optical element with a conical as opposed to spherical surface of paraxial lenses. The imaging optics are chosen such that a particle on the optical axis and in the focal plane produces a plane wave. If a microscope is used, a convex lens must be placed to "re-image" the particle image normally recorded by the imaging sensor of a camera. When the particle wavefront passes through the axicon, it is transformed into a Bessel beam which then travels free of diffraction to the camera (Durnin and Miceli 1987). Small changes in the position of the particle will produce corresponding changes in the curvature and direction of the wavefront leaving the imaging optics. Changes in curvature and direction will modify the frequency and location of the Bessel beam as seen by the camera (Snoeyink and Wereley 2012). These changes can then be related to the position of the particle using a simple algebraic relation.

This measurement technique offers several advantages over others. The first is that Interference-PTV relies on fluorescent particles small enough to be considered point sources of light. The maximum size of a particle is a

function of the imaging optics, but for an objective with a magnification of 20× particles smaller than 2 μm is ideal. Additionally, this system can easily be tailored so that its dynamic measurement range matches the needs of an experiment by adjusting the optics used. Finally, this system requires no calibration.

This article will present the optical principle upon which this measurement technique is based as well as the data analysis used to determine the properties of the Bessel beam imaged by the camera. Experimental verification of the theory will be presented, and finally, we will demonstrate the application of this measurement technique as the imaging component in a μPTV system by measuring Poisueille flow in a rectangular channel.

2 Measurement principle

Let the imaging system be generalized to a single convex lens of focal length f. This lens will transform an object point source located close to the optical axis into an image point source whose distance is given by the well known paraxial thin lens equation:

$$\frac{1}{S_o}+\frac{1}{S_i}=\frac{1}{f} \tag{1}$$

where S_o is the distance of the object point source from the lens and S_i is the distance of the resulting image. If one can determine the three-dimensional location of the point source image then it is straightforward to determine the three-dimensional location of the object point source.

To locate the position of the image point source, an axicon with a small surface angle is placed immediately after the imaging system, currently represented by a single convex lens. An axicon is an optical element with a conical surface and is most well known for its ability to produce an approximation of a Bessel beam (Durnin and Miceli 1987), which in practical situations can travel without diffracting for extended distances. Using an axicon to locate the origin of a point source of light is a unique application of this optical element.

Using the Fresnel diffraction integral, an analytical relationship can be found between the location of a point source of light and several key parameters of the resulting light pattern produced by the axicon on an image plane as shown in Fig. 1. A rigorous study of this derivation is beyond the scope of this article, but it is sufficient for the purposes of this application to state that the light from the point source will produce an approximation of a Bessel beam shown in Fig. 2 so long as the point source is sufficiently far from the axicon and close to the optical axis. The Fresnel approximation also requires these specifications.

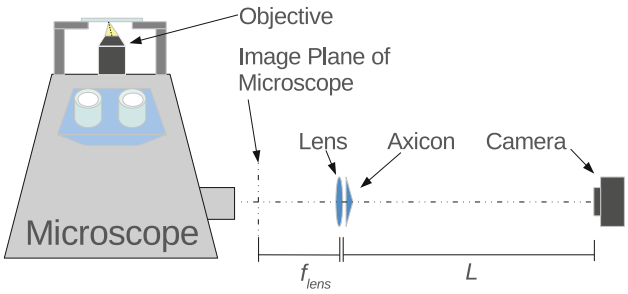

Fig. 1 Schematic demonstrating the experimental setup. Important parameters are listed

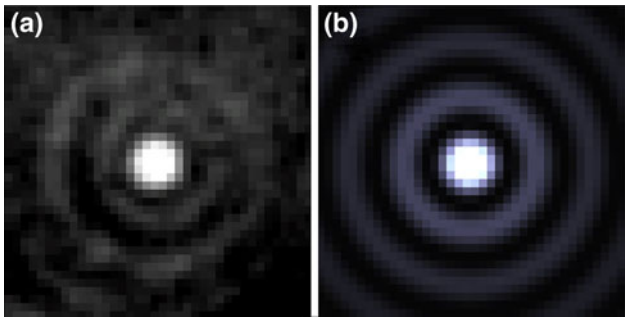

Fig. 2 An example of **a** Bessel beam produced by a fluorescent particle using the Interference-PTV experimental setup and **b** an ideal Bessel beam produced by the axicon. Note contrast and lighting have been altered to make pattern more visible

Provided the above conditions on the location of the point source are met, three properties of the Bessel beam produced can be related to the three components of the point source's location. This is accomplished by applying the following formulation of the Fresnel diffraction integral:

$$E_i(r_i,\theta_i)=\frac{-ike^{ikC}}{2\pi C}\int\int E_{ax}(r_{ax},\theta_{ax}) \times e^{\frac{ik}{C}\left[Dr_{ax}^2+Ar_i^2-2r_{ax}r_i cos(\theta_i-\theta_{ax})\right]}rd\theta_{ax}dr_{ax} \tag{2}$$

where the subscript i indicates coordinates in the image plane, and C, D, and A are the respective components of the system matrix for the optical system in between the axicon and the image plane (Collins 1970; Goodman 2004).

As shown in Snoeyink and Wereley (2012), the intensity of the resulting pattern has the following relationship:

$$I(r_c)\propto J_0^2(\beta r_c) \tag{3}$$

where r_c is the radius from the particle pattern center, J_0 is a zero order Bessel function of the first kind, and β is the

frequency of the Bessel function. The frequency of the Bessel function can be related to the point source distance with the following relationship:

$$z_p \approx \frac{\beta z_i}{k\alpha(n-1)-\beta} \tag{4}$$

where α is the angle of the axicon and n is the axicon's index of refraction, and z_i is the distance between the axicon and the imaging plane as seen in Fig. 3. Additional optical elements can be added between the axicon and camera to modify the performance of the system. If the optical system in between the axicon and image plane can be described as a system matrix using the ray transfer matrix method (Goodman 2004) then the diffraction integral can be reformulated using the system matrix formulation of the Fresnel diffraction integral (Collins 1970). Re-deriving Eq. 4 provides the following slightly modified relationship:

$$z_{point} \approx \frac{\beta C}{k\alpha(n-1)-D\beta} \tag{5}$$

where C and D refer to specific entries in the ray transfer system matrix for the optical system in between the axicon and the image plane. If there are no optical elements then $C = z_i$ and $D = 1$, which is equivalent to Eq. 4.

Once the distance to the point source has been determined, it is possible to relate the in plane location of the Bessel beam center to the in plane location of the point source:

$$x_p \approx -x_c\frac{z_p}{C} \quad x_p \approx -y_c\frac{z_p}{C} \tag{6}$$

where x_c and y_c are the x and y locations of the Bessel function center as seen in Fig. 3.

In summary, an axicon is placed between an imaging system, here simplified to a single convex lens, and a camera to locate a point source imaged by the lens. The axicon-lens combination transforms the light from the point source image into an approximation of a Bessel beam. Given the frequency and location of the center of the Bessel beam image, it is possible to use Eqs. 5 and 6 to determine the point source image location. Once the location of the point source image is known, it is a simple process to use paraxial optics to determine the location of the point source object in three dimensions provided the optical components of the imaging system are known.

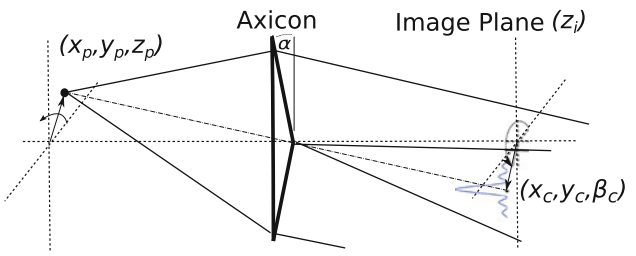

Fig. 3 Schematic demonstrating parameters used in derivation of particle pattern

This derivation has imposed two requirements on our imaging system and particles. The first requirement is that all light rays are paraxial. In practice, this implies that any point source being imaged must be relatively close to the focal plane of the imaging optics and close to the optical axis. Finally, the particles must be approximately point sources of light. This imposes an upper limit on the size of the particle used. In addition, the particles must be fluorescent with the excitation light filtered out to ensure that there is enough contrast between the particles and background.

These are, however, the only restrictions imposed on the system. For example, the size of the particle is irrelevant so long as it is small enough to be considered a point source and large enough that the camera receives enough light to discern the Bessel beam pattern. As a result, there can be considerable uncertainty in the particle size without translating that uncertainty to the particle position. In addition, the brightness of the particle is not important since this will not affect the frequency of the Bessel beam. Large variations in illumination intensity across the measurement volume will not affect the measurements provided, again, that there is enough light to discern the Bessel beam pattern.

2.1 Data analysis

2.1.1 Overview

In order to calculate the three-dimensional location of a particle, it is necessary to determine three properties of the Bessel beam imaged by the camera: both the x and y location of the Bessel beam center and the frequency of its constitutive Bessel function as shown in Eq. 3. Finding the frequency of the base Bessel function is not a trivial task, as Fig. 2 demonstrates the signal-to-noise ratio for the Bessel beam pattern can be quite low. The data analysis algorithm presented here corresponds to the optimal combination of accuracy, speed, and robustness with respect to input parameters and image noise and artifacts.

Broadly, this algorithm can be broken down into three sub-routines: a normalized cross-correlation, correlation peak finding, and maximization of the cross-correlation peak. A window is rastered across the image, and these three steps are completed at each stop in the rastering process. Information is recorded at each step and is used later to determine whether the result corresponds to a particle and is an accurate estimate of a particle's properties.

2.1.2 Normalized cross-correlation

The normalized cross-correlation example is provided in Fig. 7 and presented as Eq. 7:

$$\hat{f}\bigstar\hat{g} = \mathcal{F}^{-1}\left(\frac{\mathcal{F}(f-\overline{f})}{n\,m\sigma_f}\cdot\frac{\mathcal{F}(g-\overline{g})}{\sigma_g}\right) \tag{7}$$

where $\mathcal{F}$ denotes the discrete Fourier transform, f is the image window, $\overline{f}$ is its average and σ_f is its standard deviation, m and n are the dimensions, in pixels, of the window, and g is the ideal Bessel beam image. As can be seen in Fig. 4, a peak will form in the cross-correlation where there is a Bessel beam pattern in the image. The height of this peak is proportional to the degree of correlation between the ideal Bessel beam image and the pattern created by the particle.

The size of the window chosen for the normalized cross-correlation is important. It was found that too large a window resulted in less defined peaks due to the limited extent of the Bessel patterns. Windows that were too small, typically on the order of the width of the central peak, also had poorly defined peaks because not enough information about the Bessel beam pattern was included. Since the frequency of the Bessel beam pattern is not known *a priori*, an attempt must be made to accommodate the most extreme scenario. For the lowest spatial frequency of 0.2 pixel$^{-1,}$ the second zero of the Bessel pattern occurs at a radius of about 25 pixels. Thus, the minimum window size that would completely resolve the first lobe for the lowest frequency Bessel beam pattern is a 50 × 50 pixel window. This window is then zero-padded to twice its size before the Fourier transform step to avoid aliasing effects.

2.1.3 Correlation peak finding

The peak is located by first finding the maximum pixel in the cross-correlation and then finding the center of mass of all the pixels in a 5 × 5 window centered on it. The center of mass method is more appropriate in this application due to the relatively broad peaks encountered. More common sub-pixel peak finding methods, such as Gaussian fitting, will tend to experience significant peak locking under these conditions (Raffel et al. 2007). Once the center of mass is determined with sub-pixel accuracy, then the height of the peak is found using bi-cubic interpolation. The height and location of the peak are recorded as well as a measure of the sharpness of the peak. The smaller of the second-order finite differences with respect to either x or y of the peak is used as a metric of the sharpness of a peak. A higher second-order finite difference correlates well with the quality of a Bessel beam image.

2.1.4 Optimization

The final step is the maximization of the cross-correlation peak. The first two steps are repeated for different ideal Bessel beam frequencies until the cross-correlation peak reaches a maximum. As shown in Fig. 5, the collection of cross-correlation peaks as a function of Bessel beam frequency shows a well-behaved maximum. Since the peak is well behaved, several steps are taken to speed up the process of finding the maximum. First, the range of possible Bessel beam frequencies is discretized, and the Fourier transforms of the corresponding ideal Bessel beam images are pre-computed and stored for easy access. Then, an optimization algorithm is used to find the maximum peak.

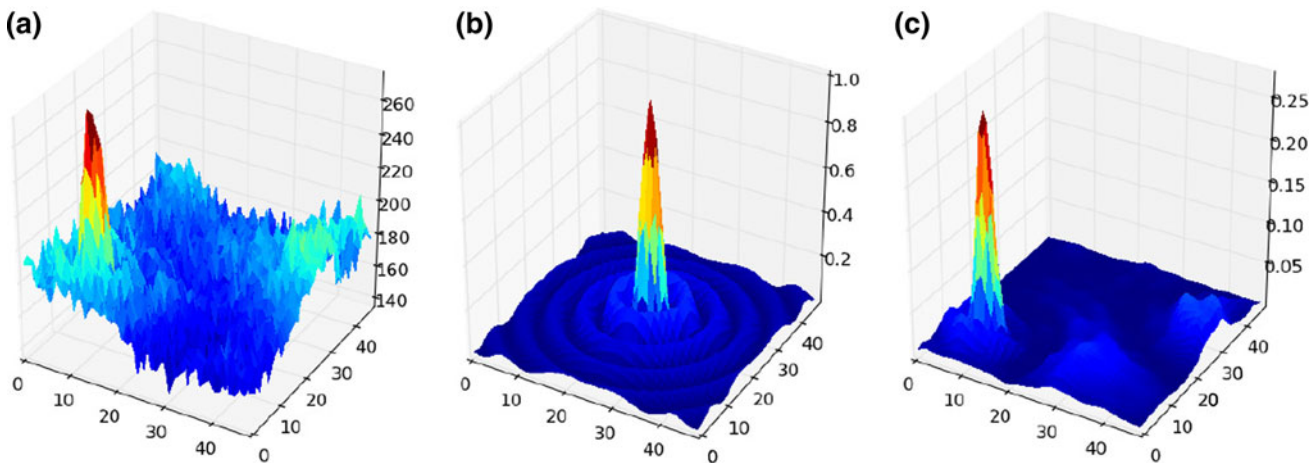

Fig. 4 Example cross-correlation. **a** An example Bessel beam image, **b** is an idealized Bessel beam Image of a particular frequency, and **c** is the result of the cross-correlation

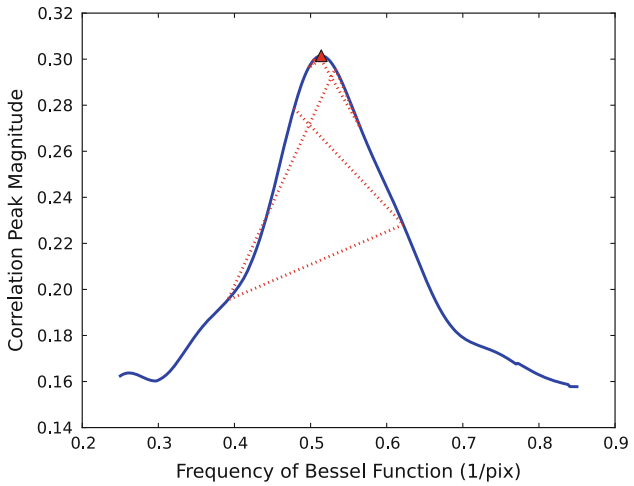

Fig. 5 An example collection of cross-correlation peaks for a range of ideal Bessel beam frequencies. *Solid line* is the collection of all possible frequencies, and the *dashed line* is the path the optimization algorithm took to find the maximum

Optimization is achieved using the golden section search method. The golden section search method is best suited for one-dimensional optimization of unimodal functions, an example of which is shown in Fig. 5. This optimization method iteratively samples the function, discarding portions of the sample space that are smaller than the current function value (Heath 2002). This optimization method is safe in the sense that it is guaranteed to complete in a fixed number of steps if the search space is discrete. Because of this feature, the range of the frequency of the ideal Bessel beam, β is broken into 256 points. This guarantees that the algorithm will converge in at most 8 iterations and with an accuracy of less then 0.5 % of the measurement range. The range of frequencies is chosen from 0.9 pixel^{-1} to 0.2 pixel^{-1}. Once the maximum frequency is found, a Gaussian is fit to the peak to find the height and frequency with sub-interval accuracy. The height and standard deviation of the Gaussian fit are both used to evaluate the quality of the data point.

2.1.5 Criteria for acceptance

For each raster location, this algorithm returns the following parameters: location of cross-correlation peak maximum (x_c, y_c), the frequency of ideal Bessel beam image at maximum β, height of maximum h, the standard deviation of Gaussian peak fit σ_{peak}, and the magnitude of the second derivative of the cross-correlation peak evaluated at the maximum κ. These values are stored and then used later to evaluate whether, in fact, there was a particle in that window. The criteria used are a series of thresholds and an empirically determined formula combining several of these parameters:

$$\beta_{\min} < \beta < \beta_{\max} \tag{8}$$

$$h_{\min} < h \tag{9}$$

$$\sigma_{\min} < \sigma \tag{10}$$

$$\kappa_{\min} < \kappa \tag{11}$$

$$C_{\min} < |h|^{\beta} \left| \frac{\kappa}{\beta} \right|^{\frac{1}{\beta}} \tag{12}$$

where $C_{\min}$ is a constant that can be adjusted to change the exclusivity of the algorithm and is found empirically.

2.1.6 Mapping the particle image to particle location

Once a particle has passed inspection, the frequency β and center (x_c, y_c) of the Bessel beam pattern are translated into the location of the particle image produced by the imaging optics using Eqs. 4 and 6. Once the location of the particle image is determined, the physical location of the particle is found by paraxial ray tracing through the imaging optics. It is notable that it is possible to run this algorithm without calibration provided with relatively easy to obtain knowledge of the imaging optic components and distances.

3 Experiments

Validation of this experimental method was accomplished by changing the distance from the focal plane of 1-μm fluorescent particles in a systematic way and comparing the calculated particle heights to the known height changes. Red fluorescent Fluorosphere particles from Invitrogen were dried on a glass microscope slide and imaged on an Axio Observer Z.1 microscope manufactured by Carl Zeiss AG using a EC Plan-Neofluar objective lens from Carl Zeiss with a magnification of 20×. Illumination was accomplished using a 2.5 W DPSS laser operating at 523 nm. The camera used was a 12 bit, 1,376 × 1,040 pixel^2, interline transfer CCD camera (Sensicam QE, PCO GmbH).

To image the particle, images produced by the microscope the following optical elements, all 1 inch in diameter, were used: a 200-mm focal length lens in the image plane of the microscope, 241 mm farther along the optical axis was an axicon with a surface angle of 0.5°, 25 mm after that was a −100-mm focal length lens followed by a 80-mm focal length lens 28 mm beyond that. The distance between the last lens and the imaging sensor of the camera was 268 mm. The Axio Obeserver Z.1 has a tube lens with a focal length of 165.4 mm separated from the objective by a distance of 100 ± 5 mm. Since the location of rear principle plane of the microscope objective is not known,

the distance from the tube lens to the microscope objective has some uncertainty associated with it.

To verify the basis of Interference-PTV, the depth of the 1-μm fluorescent particles was varied in 2-μm increments through a total depth of 100 μm giving a total measurement volume of 120 μm × 150 μm 100 μm. For this experiment, an attempt was made to replicate the conditions in an actual flow measurement. To do this, the exposure time for the camera was set to 6 ms, similar to the exposure time used in the flow measurements presented in Fig. 7.

The calculated position of the particles is plotted against the depth of the Z stage of the microscope in Fig. 6. An average of 40 particles were observed at each depth with an average standard deviation in their height of 4.2 μm, a variation that is about 4 % of the total measurement depth. Finally, a line fit to the plotted particle depths has a slope of 1.03, demonstrating a nearly 1:1 correspondence between calculated and actual changes in particle height. This fitted line, however, does not intercept the *y*-axis at zero because the Z stage height information is not zeroed on the focal plane.

The results of Fig. 6 demonstrate several advantages of Interference-PTV. The first advantage is the relatively thick measurement volume, 100 μm in this case. This distance can be extended or narrowed at will through the manipulation of any of the parameters in Eq. 5, for example, by switching from an axicon of 0.5° to one of 1.0° will result in a doubling of the effective measurement volume. It should be noted that the observable range of β remains constant. Thus, if the measurement volume is doubled, the accuracy of the measurement will decrease by a corresponding amount.

However, Fig. 6 also demonstrates a current weakness of Interference-PTV, namely that the accuracy of this technique is highly dependent on the amount of light collected from a particle. Since the information on the particle depth is spread out over the area of the Bessel beam pattern, one can increase the accuracy of the Bessel beam frequency estimation by viewing a larger pattern with more rings or with higher signal-to-noise ratio. Both of these require more light from the particles.

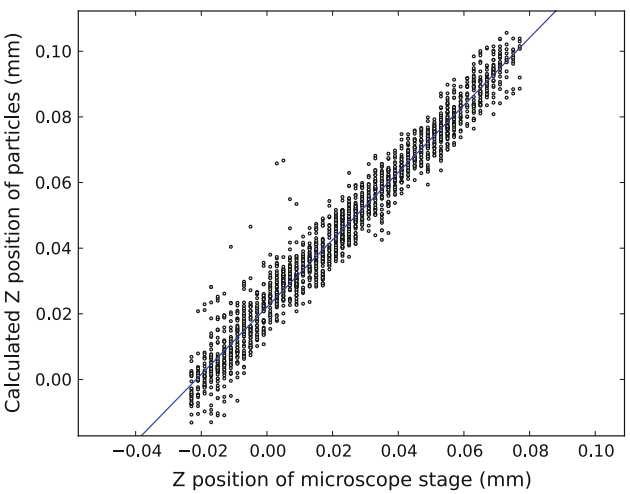

Fig. 6 Plot of calculated particle depth against depth of microscope Z stage. *Blue line* is linear curve fit to plotted particle positions with a slope of 1.03

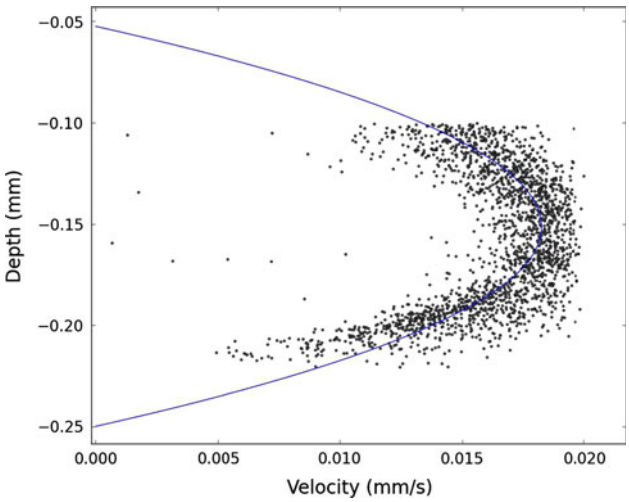

Fig. 7 Interference-PTV measurements of Poiseuille flow in 200-μm-deep microchannel. Data points are the depth of a velocity vector plotted against its magnitude. *Solid line* is a parabola fitted to the plotted data points

To demonstrate the application of this measurement method, velocity measurements were made of pressure driven flow in a microchannel using the same experimental setup described for the measurements shown in Fig. 6. The depth of the channel was 200 μm, the flow was seeded with 1 μm red fluorescent particles, and the volume flow rate was unknown. One hundred and fifty images were recorded at a frequency of 30 Hz, resulting in 2,116 velocity vectors, which were obtained using a simple nearest neighbor PTV algorithm. The magnitude of the velocity vectors is plotted against the depth of the vector in Fig. 7. This flow is steady and laminar, so a moving average of the 20 preceding images was subtracted from the each image to remove static particles and persistent noise.

As demonstrated in Fig. 6, the usable measurement depth of this experimental setup was about 100 μm; here, covering a span that includes the middle of the channel. The solid line indicates a fitted parabola, the expected velocity profile for Poiseuille flow with a coefficient of determination of 0.51. While the actual magnitude of the flow velocity is not known, the fitted line is extended beyond the plotted measurements to demonstrate that the measured section of flow does indeed correspond to Poiseuille flow in a 200-μm-deep channel. The intercepts for the fitted parabola are 197 μm apart, indicating that in

plane position, measurements in Interference-PTV have very little systematic bias due to changes in depth.

Interference-PTV can also be applied to complex three-dimensional flows such as an electrothermal vortex, a microfluidic phenomena well described and characterized by Kumar et al. (2010a). The electrothermal vortex is a microfluidic phenomenon that occurs when an alternating voltage is applied to two parallel electrodes that are separated by a fluid filled gap and a spatially located heat source is applied to the fluid. The resulting permittivity and conductivity variations caused by temperature gradient result in a body force when subjected to the alternating electric field. The body force causes a flow that result is a three-dimensional toroidal vortex centered on the heat source (Kumar et al. 2010b). Particles entrained in the flow can follow complex three-dimensional paths through the vortex, an ideal system in which to demonstrate three-dimensional particle tracking.

One such particle was tracked in an electrothermal vortex formed in a 50-μm gap using a 3.5 V peak to peak AC voltage driven at 10 kHz. Figure 8a shows the path of this particle as well as the magnitude of its velocity. A 1° axicon was used for these experiments with a 40× lens. The resulting measurement volume is about 150 μm thick, or three times greater then the thickness of the flow field measured. The particle track was still recorded with a max velocity in the region of 100 $\frac{\mu m}{s}$.

For comparison, measurements of the same electrothermal vortex phenomena performed using astigmatism PTV are provided in Fig. 8b. These two measurements were performed under different conditions, so it is not possible to quantitatively compare these two measurements. However, there are several qualitative similarities. The Interference-PTV measurements clearly show the vortex structure demonstrated in the astigmatism PTV measurements. Additionally, both measurements show an increasing velocity magnitude as the particles travel in spirals with a smaller radius.

3.1 Particle considerations

Particle size is typically an important factor in particle-based velocimetry methods, and Interference-PTV is no different. The actual particle image is the convolution of the particle intensity profile and the PSF of the microscope, in this case a Bessel beam as seen in Eq. 3. Since it is the spatial frequency of this Bessel beam that is used to determine the depth of the particle, it is important that the image of the particle does not overwhelm the PSF.

This issue is particularly relevant for particles that are far from the microscope objective. In this case, as per Eq. 4, the spatial frequency of the Bessel beam increases and the spacing of the interference rings decreases. Since the width of the PSF central peak is quite small, the image of the particle must also be very small to prevent aberrations in the Bessel pattern. As a result, the authors recommend using particles which have a projected image size of less then 4 pixels in diameter. As an example, for a system with 20× magnification and a camera pixel size of 7.4 μm, this would limit the particle size to less than 1.5 μm.

If it is not possible to choose particles that are small enough to satisfy the above rule then the results can be unpredictable. The algorithm presented here does not fail

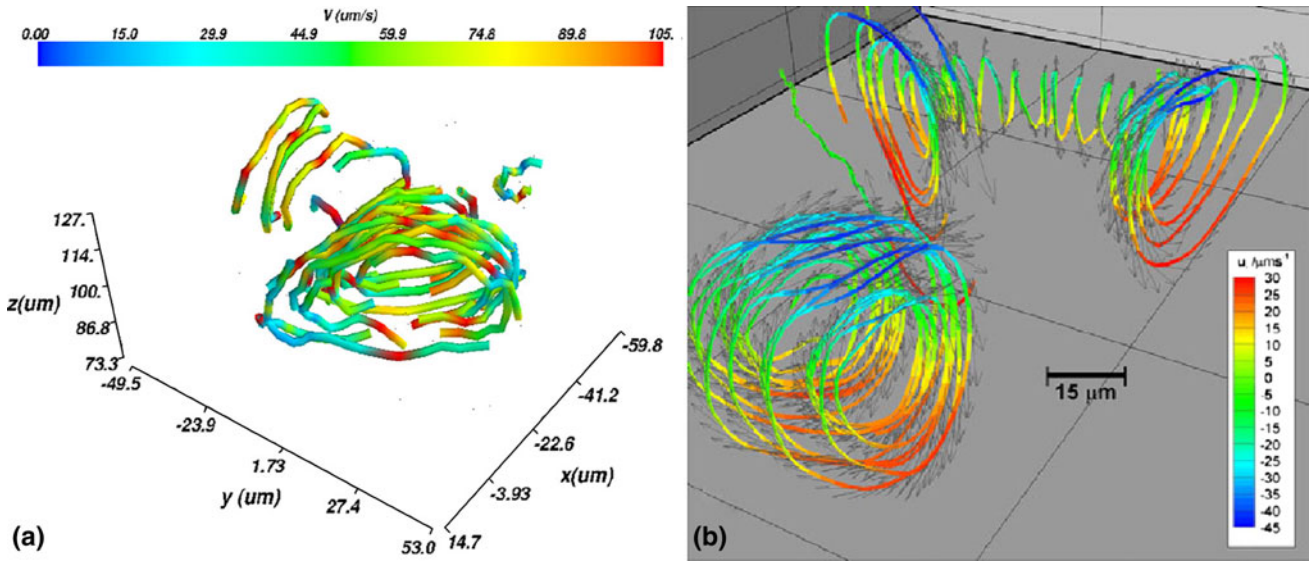

Fig. 8 Three-dimensional PTV measurements of two different electrothermal vortex using: **a** Interference-PTV and **b** astigmatism PTV reprinted with permission from Kumar et al. (2010a)

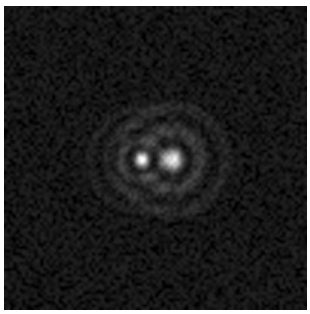

Fig. 9 Simulated image of two Bessel patterns offset by 8 pixels. *Left* pattern has a spatial frequency of 0.6 pixels$^{-1,}$ and *right* pattern has a spatial frequency of 0.4 pixels^{-1}

gradually with increasing uncertainty as the particle size increases. Instead, the algorithm accurately determines the spatial frequency until the combination of particle size and image noise is enough to obscure the PSF. At this point, the algorithm returns an effectively random response. The filters presented effectively detect these occurrences and reject them, though it can cause particles to intermittently be recognized in tracking applications and should be avoided if possible.

A second important consideration which typically has a large effect on the accuracy of three-dimensional particle tracking methods is particle concentration (Cierpka and Kähler 2011). This issue arises at large particle densities the particle images will begin to overlap. This will typically interfere with the image analysis algorithm's ability to determine key properties of the image. Interference-PTV is no different, overly dense particle concentrations can cause difficulties in analyzing individual Bessel patterns.

The algorithm described in this manuscript is capable of distinguishing and interpreting two Bessel patterns even when their side lobes are highly overlapping. Figure 9 shows an example of two simulated Bessel patterns separated by 8 pixels. The image analysis algorithm is capable of locating the particle centers to within 0.1 pixel and the spatial frequency to within 0.005 pixel^{-1}, comparable with accuracies found when analyzing individual particles. Closer than this and uncertainties in the pattern center and frequency quickly increase. While the effects of particle concentration are not explored in this manuscript, this required spacing suggests that particle concentrations on the order of several hundred particles can be accommodated by typical cameras.

4 Conclusion

A unique method of locating the three-dimensional location of fluorescent particles termed Interference-PTV is described for the first time and applied to the task of flow characterization in a microfluidic channel. By re-imaging the particle images produced by a microscope with a combination of a convex lens and axicon, the light from a particle is transformed into an approximation of a Bessel beam.

Two properties of this Bessel beam: its center (x_c, y_c) and its frequency β in the image plane of the camera are shown to be directly related to the location of the original particle provided knowledge of the optical components of the imaging system and the wavelength of light used. A robust and accurate algorithm for determining these three parameters was also described and applied toward two experiments demonstrating the validity of this measurement method. These demonstrated several advantages of Interference-PTV:

- A typical micro-PIV setup can be easily modified to be capable of Interference-PTV measurements
- The measurement volume is relatively deep and can be easily adjusted to maximize sensitivity for a given flow geometry by changing the angle of the axicon used. As a result, often times an entire microfluidic channel can be imaged without need for scanning
- Since Interference-PTV has a complete analytical relationship between particle location and the properties of the image Bessel beam, no calibration is necessary.
- Interference-PTV is insensitive to variations in particle size or to variations in particle brightness across the measurement volume and between images.

In particular, the insensitivity of this technique toward particle size and brightness and lack of calibration is unique among 3D-PTV techniques that rely on the particle image. This provides an advantage in situations in which the size or brightness of the particles varies significantly or is not known ahead of time. Alternatively, this Interference-PTV is well suited to situations where non-uniformity in illumination cannot be controlled for in the experiment.

It should also be noted that this technique is not limited to microscopes, though it finds its greatest utility in situations where multi-view three-dimensional techniques are not possible. This technique can be applied to any optical imaging system where small light sources with high contrast must be located in three dimensions.

Acknowledgments Thank you to Prof. Dr. Christian Kaehler for his generous support over the summer. We would also like to extend our gratitude to Dr. Christian Cierpka, Dr. Massi Rossi, and Rodgrigo Seguro for their time and invaluable guidance.

References

Choi YS, Seo KW, Sohn MH, Lee SJ (2012) Advances in digital holographic micro-PTV for analyzing microscale flows. Opt Lasers Eng 50(1):39–45

Cierpka C, Kähler CJ (2011) Particle imaging techniques for volumetric three-component (3D3C) velocity measurements in microfluidics. J Vis 15(1):1–31

Cierpka C, Segura R, Hain R, Kähler CJ (2010) A simple single camera 3C3D velocity measurement technique without errors due to depth of correlation and spatial averaging for microfluidics. Meas Sci Technol 21(4):045401

Cierpka C, Rossi M, Segura R, Kähler CJ (2011) On the calibration of astigmatism particle tracking velocimetry for microflows. Meas Sci Technol 22(1):015401

Collins J (1970) Lens-system diffraction integral written in terms of matrix optics. J Opt Soc Am 60(9):1168–1177

Durnin J, Miceli JJ (1987) Diffraction-free beams. Phys Rev Lett 58(15):1499–1501

Goodman JW (2004) Introduction to fourier optics, 3rd edn. Roberts & Co., Englewood

Katz J, Sheng J (2010) Applications of holography in fluid mechanics and particle dynamics. Annu Rev Fluid Mech 42(1):531–555

Kim S, Lee SJ (2007) Measurement of 3D laminar flow inside a micro tube using micro digital holographic particle tracking velocimetry. J Micromech Microeng 17(10):2157–2162

Kumar A, Cierpka C, Williams SJ, Kähler CJ, Wereley ST (2010a) 3D3C velocimetry measurements of an electrothermal microvortex using wavefront deformation PTV and a single camera. Microfluid Nanofluid 10(2):355–365

Kumar A, Kwon JS, Williams SJ, Green NG, Yip NK, Wereley ST (2010b) Optically modulated electrokinetic manipulation and concentration of colloidal particles near an electrode surface. Langmuir 26(7):5262–72

Lindken R, Rossi M, Große S, Westerweel J (2009) Micro-particle image velocimetry (PIV): recent developments, applications, and guidelines. Lab Chip 9(17):2551

Lu J, Pereira F, Fraser SE, Gharib M (2012) Three-dimensional real-time imaging of cardiac cell motions in living embryos. J Biomed Opt 13(1):014006

McLeod JH (1954) The axicon: a new type of optical element. J Opt Soc Am 44(8):592

Meinhart CD, Wereley ST, Santiago JG (1999) PIV measurements of a microchannel flow. Exp Fluids 27(5):414–419

Heath MT (2002) Scientific computing: an introductory survey. McGraw-Hill, New York

Nguyen CV, Carberry J, Fouras A (2011) Volumetric-correlation PIV to measure particle concentration and velocity of microflows. Exp Fluids 52(3):663–677

Olsen MG, Adrian RJ (2000) Out-of-focus effects on particle image visibility and correlation in microscopic particle image velocimetry. Exp Fluids 29(7):S166–S174

Raffel M, Willert CE, Wereley ST, Kompenhans J (2007) Particle image velocimetry: a practical guide. Springer, Berlin

Santiago JG, Wereley ST, Meinhart CD, Beebe DJ, Adrian RJ (1998) A particle image velocimetry system for microfluidics. Exp Fluids 25(4):316–319

Satake Si, Kunugi T, Sato K, Ito T, Kanamori H, Taniguchi J (2006) Measurements of 3D flow in a micro-pipe via micro digital holographic particle tracking velocimetry. Meas Sci Technol 17(7):1647–1651

Snoeyink C, Wereley S (2012) Three-dimensional locating of paraxial point source with axicon. Opt Lett 37(11):2058

Sohn MH, Seo KW, Choi YS, Lee SJ, Kang YS, Kang YS (2010) Determination of the swimming trajectory and speed of chain-forming dinoflagellate Cochlodinium polykrikoides with digital holographic particle tracking velocimetry. Mar Biol 158(3):561–570

Speidel M, Jonás A, Florin EL (2003) Three-dimensional tracking of fluorescent nanoparticles with subnanometer precision by use of off-focus imaging. Opt Lett 28(2):69–71

Wereley ST, Meinhart CD (2010) Recent advances in micro-particle image velocimetry. Annu Rev Fluid Mech 42(1):557–576

Wu M, Roberts JW, Buckley M (2005) Three-dimensional fluorescent particle tracking at micron-scale using a single camera. Exp Fluids 38(4):461–465

Yoon S, Kim K (2006) 3D particle position and 3D velocity field measurement in a microvolume via the defocusing concept. Meas Sci Technol 17(11):2897–2905